Neuroradiology (1990) 31: 512-522

Neuro radiology

Occult spinal dysraphism: neuroradiological study

P. Tortori-Donati [1], A. Cama [2], M.L. Rosa [1], L. Andreussi [2], and A. Taccone [3]

[1] Department of Neuroradiology, Ospedale San Martino, and Departments of [2] Neurosurgery and [3] Radiology, Istituto G. Gaslini, Genova, Italy

Summary. We present a retrospective study of occult spinal dysraphism in 47 children aged 0 to 14 years, all studied with plain X-rays, 60% with CT and myelo-CT, and 40% with MR. We consider the classification and grading of these malformations, clinical, neuroradiological patterns, and indications for surgery. In the light of our findings and of the published data MR emerges as the key investigation. Only in a few cases of great anatomical complexity is it now necessary to perform CT and myelo-CT as well. A case in point is when the conus and thickened filum terminale are inextricably bound together and can no longer be considered separate structures. We propose the term "neurofibrous structure" to define the conus-thickened-filum-terminale unit when these structure are no longer distinguishable.

Key words: Occult spinal dysraphism - Lipoma - Tethered cord - Spinal cord - Caudal regression syndrome - Developmental mass lesions

The clinical and radiological diagnosis of spinal dysraphism has always been a difficult matter, both because of the age of onset and because of the complexity of the lesions. The improvement brought about by CT and by myelo-CT [1-4] scanning in the neuroradiological diagnosis of spinal dysraphism has been heightened by the advent of magnetic resonance (MR) [5-16]. But althought MR alone often provides a complete diagnosis, in some cases the information supplied by myelo-CT scans affords a more precise assessment of the interrelationships contracted by the various components of the malformation [17].

We shall here describe our experience in the diagnosis of occult spinal dysraphism (OSD) and associated developmental mass lesions.

Definition and classification

Spinal dysraphisms are embryopathies comprising a wide range of heterogeneous central nervous system (CNS) abnormalities characterized by imperfect differentiation and fusion of the dorsal midline structures: skin cover and aponeurotic muscle, spine, meninges and neural structures [1, 18-20]. This group of malformations includes:

Spina bifida aperta. Dorsal herniation of all or part of the spinal contents (meningocele, myelomeningocele, myeloschisis).

Occult spinal dysraphism. The malformation is covered by skin and does not expose neural tissue or obvious cystic masses, which, when present, are attributable to lipoma (asymptomatic spina bifida occulta, lipoma, lipomyelomeningocele, diastematomyelia, dermal sinus, developmental mass lesions, tethered cord syndrome, split nothocord syndrome, caudal regression syndrome, spina bifida anterior).

Embryology

Spinal dysraphisms are the outcome of incomplete fusion of the neural tube and occur at various stages of embryogenesis [21, 22]. The anomalous or defective fusion of one or more layers gives rise to various anatomical types of spinal dysraphism, which varies with the importance of the structures involved, the level and time of onset during embryogenesis.

The formation of the spinal cord and its meninges is the end-result of successive reciprocal stimuli beginning with the neural plate. Any disturbance of these stimuli at any stage of embryogenesis causes dysraphisms, whose severity will depend on the precocity and extent of the lesion [22].

The sequestration of normal tissue constituents during fetal development and their subsequent

Table 1. Summary of cases and correlation between some different forms of spinal dysraphism

	N°	Dermal sinus	Tethered cord
Lipomas	21	5	20
Lipomyelomeningoceles	10	1	10
Dermoids	11	9	5
Teratomas	2	/	1
Diastematomyelia	2	/	1
Caudal regression s.	1	/	/
Total	47	15	37

growth will lead to the formation of developmental mass lesions. According to the germ layer or layers of which they consist, they will take the form of: epidermoids (ectoderm), dermoids (ecto-mesoderm), teratomas (ecto-meso-endoderm) or lipomas (mesoderm) [1, 10].

The embryological features of these lesions, often associated with dysraphic states, have led us to regard them as actual occult spinal dysraphisms.

Patients and method

In the Pediatric Neurosurgery Service of Istituto G. Gaslini, Genova, we have in the past ten years seen 47 patients with spinal dysraphisms (Table 1), their ages ranging from the neonatal period to 14 years.

All the children underwent standard radiographic examination; 60% had myelo-CT scans and since 1984 MR scans (40%). The CT scans done at the Gaslini Hospital and in the Neuroradiology Service of San Martino Hospital, Genova, were carried out on Atom 1200[1] and Somatom DR 2[2] scanners, mostly in the axial plane with subsequent reconstruction; in some cases direct sagittal scans were taken. The quantity of intrathecal contrast medium varied with patient age. MR imaging was done mainly in the San Martino Hospital Neuroradiology Service (Esatom 1500[1], 0.15 T resistive magnet unit) and at the Gaslini Hospital (Esatom 5000[2], 0.5 T superconducting magnet unit).

Spin-echo sequences with repetition times of 500, 2000 and echo times of 30/50/100 were used to obtain T1- and T2- weighted images and multi-echo sequences with a repetition time of 1500 and echo times of 30/70/120. Slice thickness was 5, 7 and 10 mm with 4–8 acquisitions. The planes for study were chosen according to the type of pathology, starting with sagittal sections, which proved to be essential. We do not use T2-weighted sequences unless indispensable because they take much longer and so are unsuitable for children who are often uncooperative or sedated. The MR investigation took from 30 to 90 minutes. Some patients arrived with the neuroradiological assessment from their local hospital.

[1] Ansaldo Esaote, Genova, Italy
[2] Siemens, Erlangen, Federal Republic of Germany

Case-material and discussion

Our patients are classified in Table 1. Most OSD require no treatment in the neonatal period. The neurological status may remain within normal limits for a long time and the patients come to observation at varying stages. Although often benign, OSD may present a downhill neurological course as time goes on, and this is unlikely to be reversed if surgical treatment is unduly delayed [23–26].

The patients were assessed clinically on the scale proposed by Hoffman [27]:
- Grade 0: neurologically normal.
- Grade 1: slight neurological deficits, minor foot deformities but no gait disturbance. Normal sphincter function.
- Grade 2: weakness of the lower limbs. Bladder normal or isolated neurological bladder.
- Grade 3: moderate lower limb deficit with gait disturbances and neurological bladder.
- Grade 4: severe paraparesis and walking only with support.
- Grade 5: paraplegia.

Eighteen patients diagnosed and treated surgically within the first year of life had been graded 0–1 and showed no clinical deterioration after the operation.

Of the 26 grade 2–3 patients operated on at a later stage 22 obtained stabilization of the clinical signs, 2 an improvement in walking and 1 experienced deterioration of sphincter function.

This group includes a few patients who were initially graded 0 or 1 and who with growth developed bladder disturbances and progressive difficulty in walking. Surgical treatment arrested progression of the symptoms. Two grade 0 patients with mild OSD did not receive surgical treatment and are being regularly monitored clinically and by laboratory and instrumental tests.

Lipomas [28–34]

Time of onset during embryogenesis: 28th–48th day.

As the table shows, the malformation most frequently associated with OSD is lipoma. It usually consists of a mass of mature fat tissue, more or less encapsulated and crossed by fibrous bands which divide it into lobules [34] (Fig. 1a, b); although the

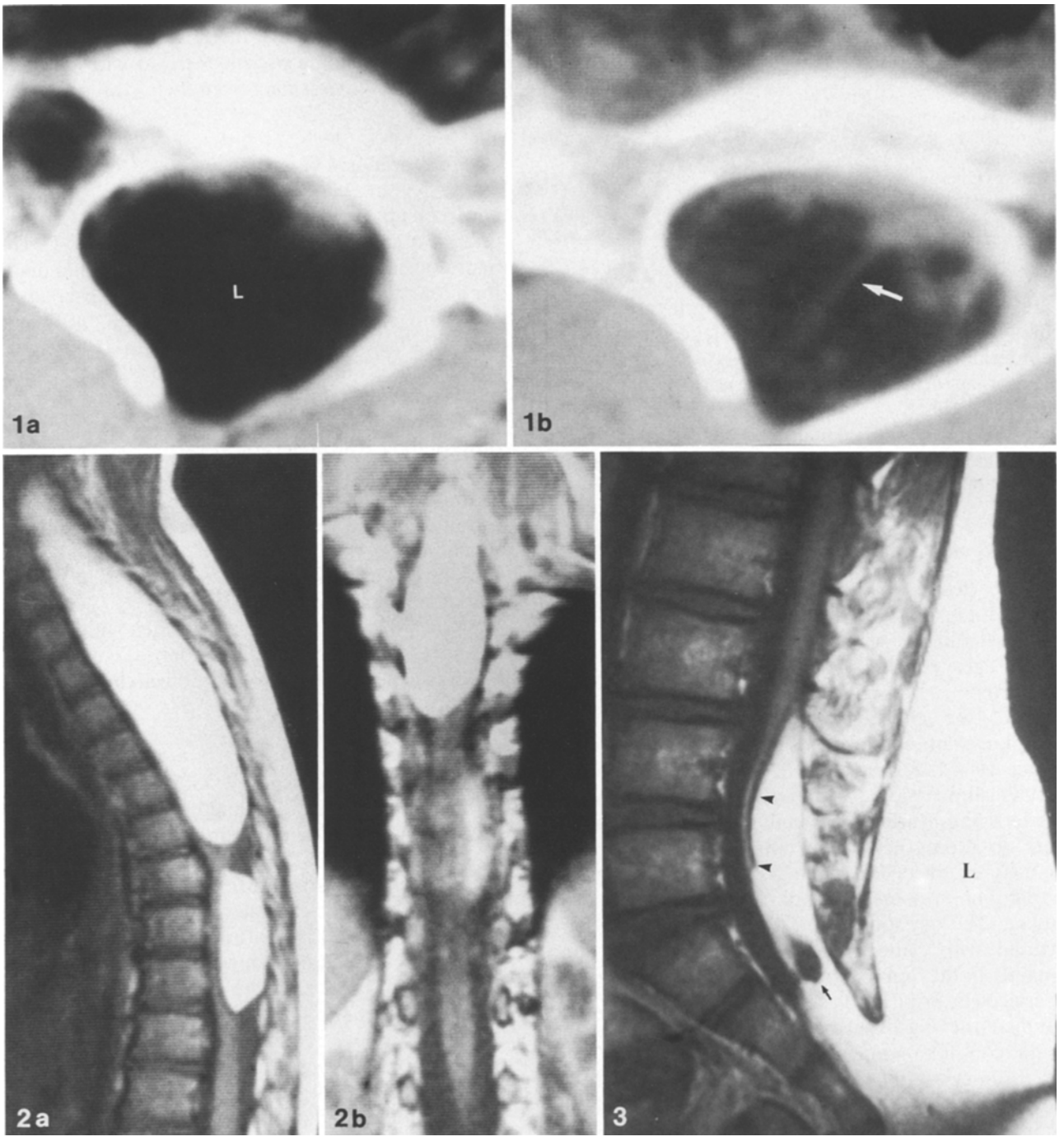

Fig. 1 a, b. Lumbosacral intradural lipoma. CT: axial scans. Markedly hypodense lesion *(L)* crossed by fibrous bands *(arrow)* which divide it into lobules. Enlarged and asymmetrical spinal canal with schisis of the posterior arch

Fig. 2 a, b. Bifocal cervicothoracic intradural lipoma. MR: SE T1-weighted TR 350 - TE 30, sagittal and coronal scans. Giant lesion with dual localization and homogeneous high signal intensity. The cranial lipoma causes pronounced widening of the spinal canal, to the detriment of the posterior arches and of the vertebral bodies, and a thoracic kyphosis. The spinal cord is imaged on the sagittal scans but appears on the coronal scans with leftward displacement. The spinal cord at the level of the caudal lipoma is still visible but is thinned and pushed against the plane of the vertebrae and discs

Fig. 3. Lumbosacral intra- and extraspinal lipoma. MR: TR 600 - TE 20, Sagittal scans. Bulky subcutaneous lipoma *(L)* which through a large cleft enters the spinal canal and subdural space. The neurofibrous structure is implanted on the lipoma after a short passage along its ventral wall *(arrow)*. The hypointense image within the lipoma is due to a CSF cyst

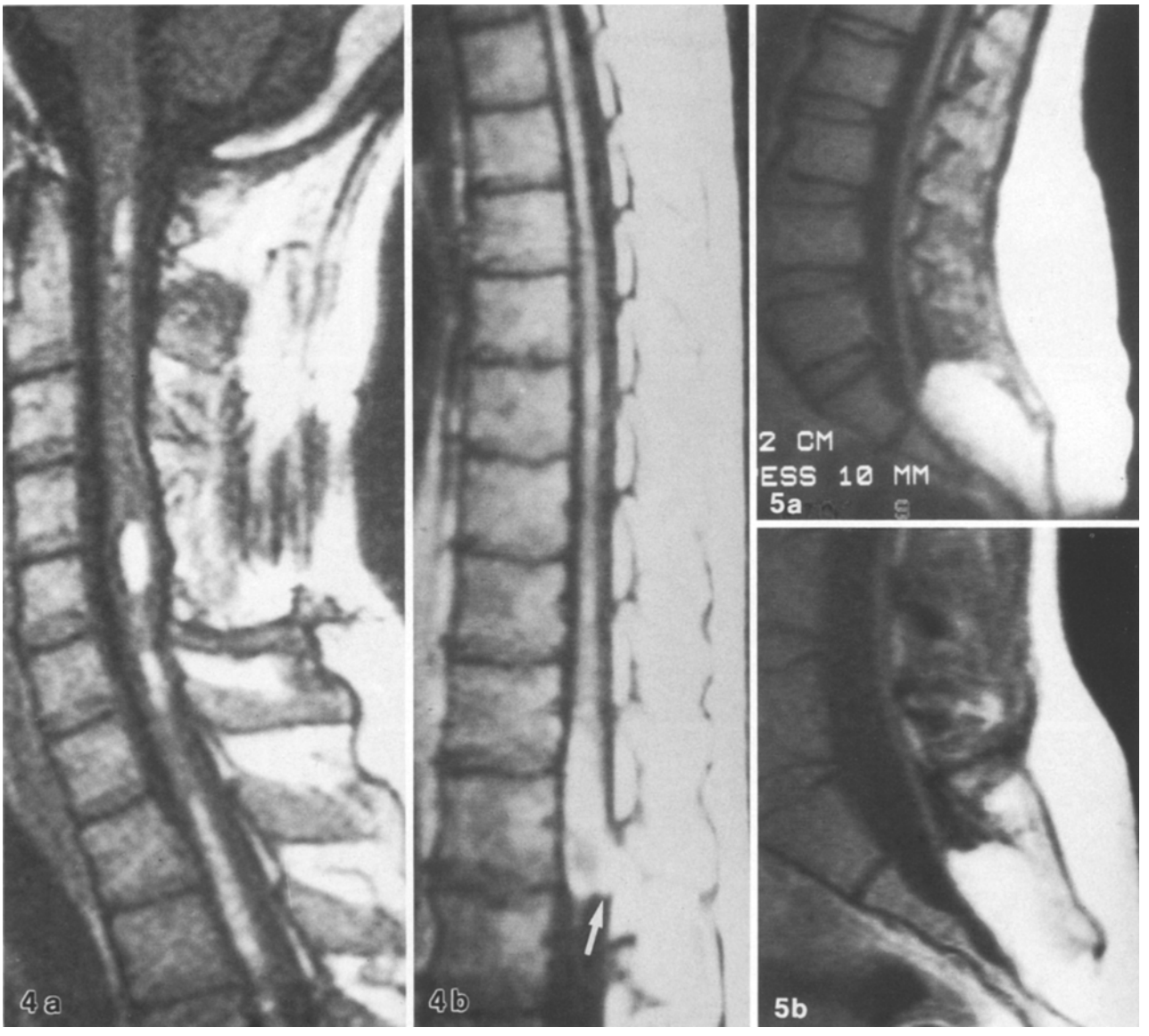

Fig. 4a, b. Diffuse lipomatosis. MR: SE T1 - weighted TR 350 TE 30, sagittal scans. Intramedullary areas of increased signal intensity. The lipoma at C4–C5 level causes swelling of the cord. At conus level the lipoma has an exophytic component that is attached dorsally to the dura mater *(arrow)*

Fig. 5a, b. Tethered cord and lumbosacral lipomas. MR: RT 500 ET 30, sagittal scans. The spinal cord runs in close contact with the spinolaminar line, from which it departs only to tether itself to the upper pole of the lipoma. Marked dilatation of the lumbosacral spinal canal

most frequent form of OSD, it accounts for less than 1% of primitive intraspinal tumors [28]. Here we shall consider the variety that Emery and Lendon [29] in their classification termed leptomyelolipomas: "A bizarre admixture of varying amounts of fat with the central nervous tissue of the spinal cord, dense connective tissue of the dura and a rather loose vascular tissue of an arachnoid type very common in association with areas of neurospinal dysraphism".

Lipomas are more commonly found at lumbosacral level [32] but may occur elsewhere along the spinal canal, sometimes being multifocal and of monstrous size (Fig. 2a, b). They may be totally intraspinal but commonly possess a subcutaneous component. Often they are only small outgrowths of a much larger extraspinal lipoma (Fig. 3). Very rarely they lie totally inside the cord with the appearance of diffuse lipomatosis (Fig. 4a, b).

They are tigthly bound to the conus and there is no true cleavage plane. Chapman [30] classified lipomas according to their position and relationship to the conus as: dorsal (Fig. 4b), transitional and caudal

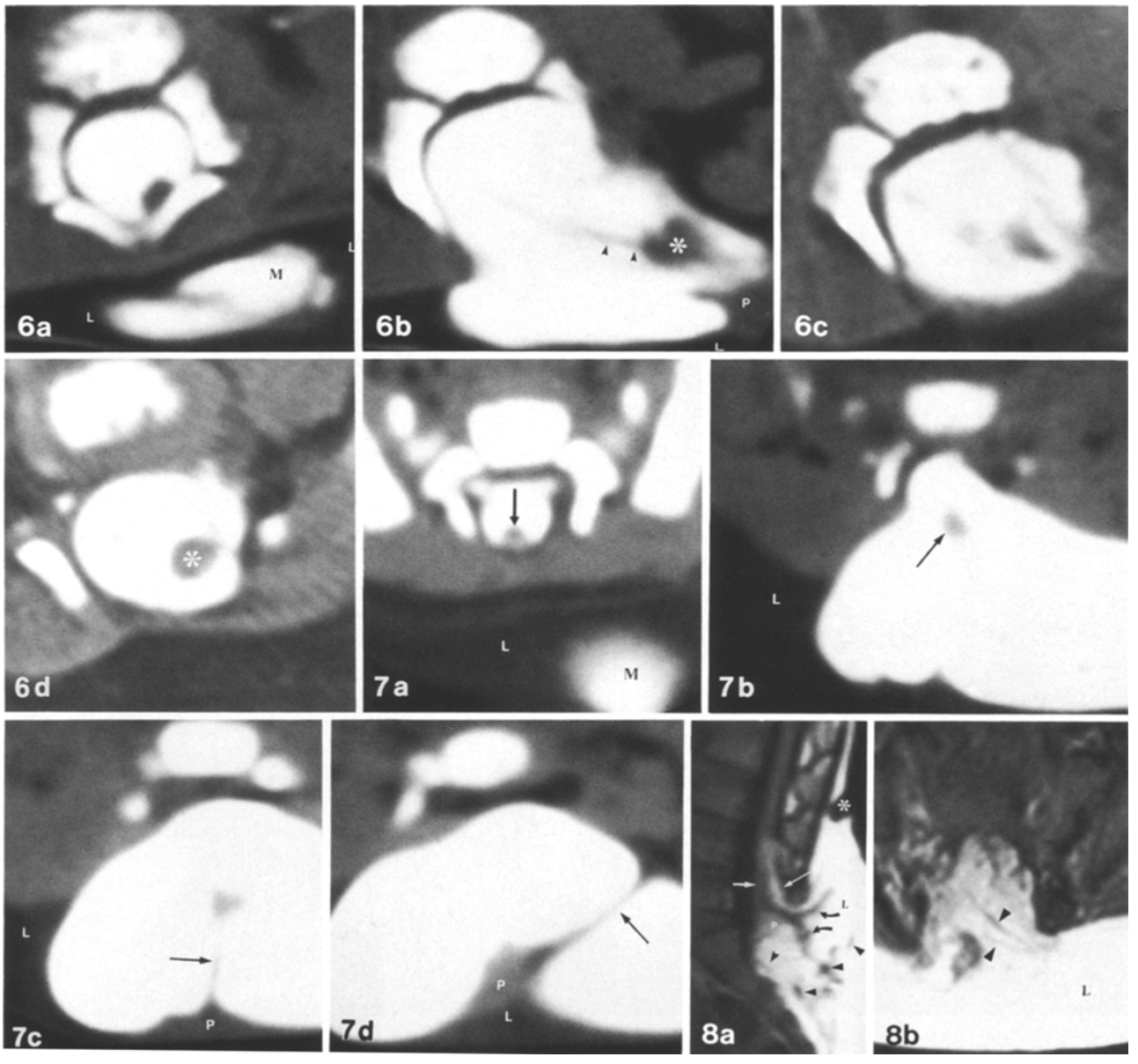

Fig. 6a–d. Lipomyelomeningocele. Myelo-CT: axial scans. **a** Spinal cord in eccentric position and in close contact with the left vertebral lamina. Upper portion of the dural sac everted *(M).* **b** Placode *(P)* and cord *(asterisk)* in eccentric position and outside the spinal canal, from where arise roots *(arrowheads)* with an abnormal course inside the dural sac *(arrows). L:* lucent dorsal lipoma. **c, d** The cord *(asterisk)* seeks to reposition itself within the spinal canal. In sum, the cord describes a left-facing convex loop on the apex of which lies the placode, site of attachment of the lipoma

Fig. 7a–d. Lipomyelomeningocele. Myelo-CT: axial scans. **a** Cord on the midline dorsally *(arrow).* Upper portion of the meningocele *(M).* **b** Cord outside the spinal canal *(arrow).* **c** Fibrous band *(arrow)* uniting the cord to the placode *(P).* **d** Fibrolipomatous band *(arrow)* starting from the neural plate, which divides the meningocele obliquely

Fig. 8a, b. Lipomyelomeningocele. MR: TR 450 - TE 30. Sagittal and axial scans. Bulky subcutaneous lipoma entering the sacral canal through a large cleft. Funnel-shaped placode *(P)* attached to the upper pole of the intradural lipomatous component, tethered cord *(white arrow),* connective-fibrous structures *(black arrowheads),* outpocketings of the dural sac *(curved arrows)* with overlying epidural adipose tissue *(thin white arrow),* zone of cutaneous depression due to dystrophic-cicatricial processes *(asterisk)*

(Fig. 5 a, b). Nearly all our patients had more or less pronounced spina bifida together with complex vertrebral malformations. The presence of malformed bone is evidence of the slow growth of these lesions.

The CT scan always shows a markedly hypodense nonenhancing area within the spinal canal, often combined with spina bifida [1, 23, 31] (Fig. 1). On the MR scan [11, 13, 14, 35] a lipoma appears as a

more or less spherical mass with an intense signal in the T1-weighted sequences, often within an abnormally enlarged lumbosacral spinal canal [12, 36]. The spinal cord is implanted on the lipoma often eccentrically and away from the spinolaminar line, thus forming one of the classic patterns of the tethered cord syndrome (Fig. 5 a, b).

Tethered cord

Time of onset during embryogenesis: from the 43rd day.

Tethered cord is an almost constant features of the embryonic malformative developmental sequence (Table 1). The conus is tethered very low by certain intradural anomalies. New procedures, especially MR, have spelled out more clearly the anatomical variants of this malformation. The most frequent radiological features are:
- Cord tethered by an intra-extradural lipoma (Figs. 3-5)
- Cord tethered dorsally by fibrous bands or by fibrolipomatosis (Fig. 4)
- Cord tethered to the base of the dura sac by a tight, thickened fibrous filum terminale (Fig. 9)
- Stretching of the thickened, fibrous or fibrolipomatous conus and tethering of it directly ot the sacrococcygeal region (Fig. 10).

Lipomyelomeningoceles [1, 4, 14, 15, 17, 23, 27]

Time of onset during embryogenesis: 28th-48th day.

Naidich has given a wonderful description [43] of the features of this class of lesion, but the problems of diagnosis and precise morphological attribution nonetheless remain rather complex. Lipomyelomeningoceles are protean lesions: the meninges are often asymmetrically everted, the cord is not always on the midline and the placode is rotated and tethered to the lipoma eccentrically (Fig. 6 a-d); fibrous bands are sometimes present on several planes of the space (Fig. 7 a-d).

It is in this type of lesion that CT scanning is a valuable complement of MR scanning. The malformation itself is not hard to diagnose but difficulties do sometimes arise regarding its precise morphology and the interrelations of its various components: cord, placode, root, meninges, lipoma, vertebral column (Fig. 8 a, b). Sagittal and coronal MR views combined with axial CT scans with water soluble contrast medium allow a more detailed analysis of the pathological anatomy.

Diastematomyelia [15, 22, 44-48]

Time of onset during embryogenesis: 16th-17th day.

Diastematomyelia is a complex malformation characterized by a segmental duplication of the spinal cord and the formation of two hemicords with a central canal and a ventral and dorsal horn giving rise to their respective roots.

The hemicords are split by a bony, fibrous or cartilaginous spicule (Diastematomyelia with septum) [47]. The most frequent site is the thoracolumbar region. Vertebral body malformations are found in 60% of cases. Diastematomyelia may be associated with abnormalities or dysmorphisms of the superficial planes and with other OSD malformations. Coronal and oblique MR scans are especially helpful in the study of this dysraphism, supplying a clear and detailed image of the site and extent of the cleft, of the morphology and dimension of the two hemicords, of their relationships with the spicule and any related malformations.

Developmental mass lesions

Of these lesions the one most often associated with OSD, after lipoma, is the dermoid. We had no case of epidermoid, probably because, developing so slowly, they do not often manifest themselves until adulthood (20-50 years) [54].

Dermoids account for some 10% of spinal tumors before the age of 15. They are due to the inclusion of ectodermal and mesodermal tissue rests and in a fair percentage of cases are associated with a dermal sinus (Table 1). The fistula, lined with stratum germinativum, extends from the skin surface to a variable depth, often contracting connexions with the spinal structures and their contents. Its course is variable but is frequently craniocaudal (72%) [24, 49], as it was in all our cases scanned with MR (Fig. 10). The terminal portion may communicate directly with a dysontogenetic lesion [50]. On CT scanning a dermoid usually images as a hypodensity of variable degree (Fig. 11 a, b), which does not always enhance on intravenous injection of contrast. Sometimes it possesses a capsule, which may enhance. Difficulties may arise in the differential diagnosis from possible intramedullary lesions, especially when they lie in the rostral portions of the spinal canal. The relationship with adjacent structures are always rather complex.

In our series the MR signal intensity pattern was similar to the CT density pattern of this malformation. The lesion "tends to conceal itself", is hypointense in the T1- (Fig. 11 c) and isohypointense versus the cord parenchyma in the T2-weighted sequences (Fig. 11 d). Accurate study of the signal, however, as a rule permits indentification of the lesion and differentiation from the neighboring structures so that a fairly clear morphology emerges.

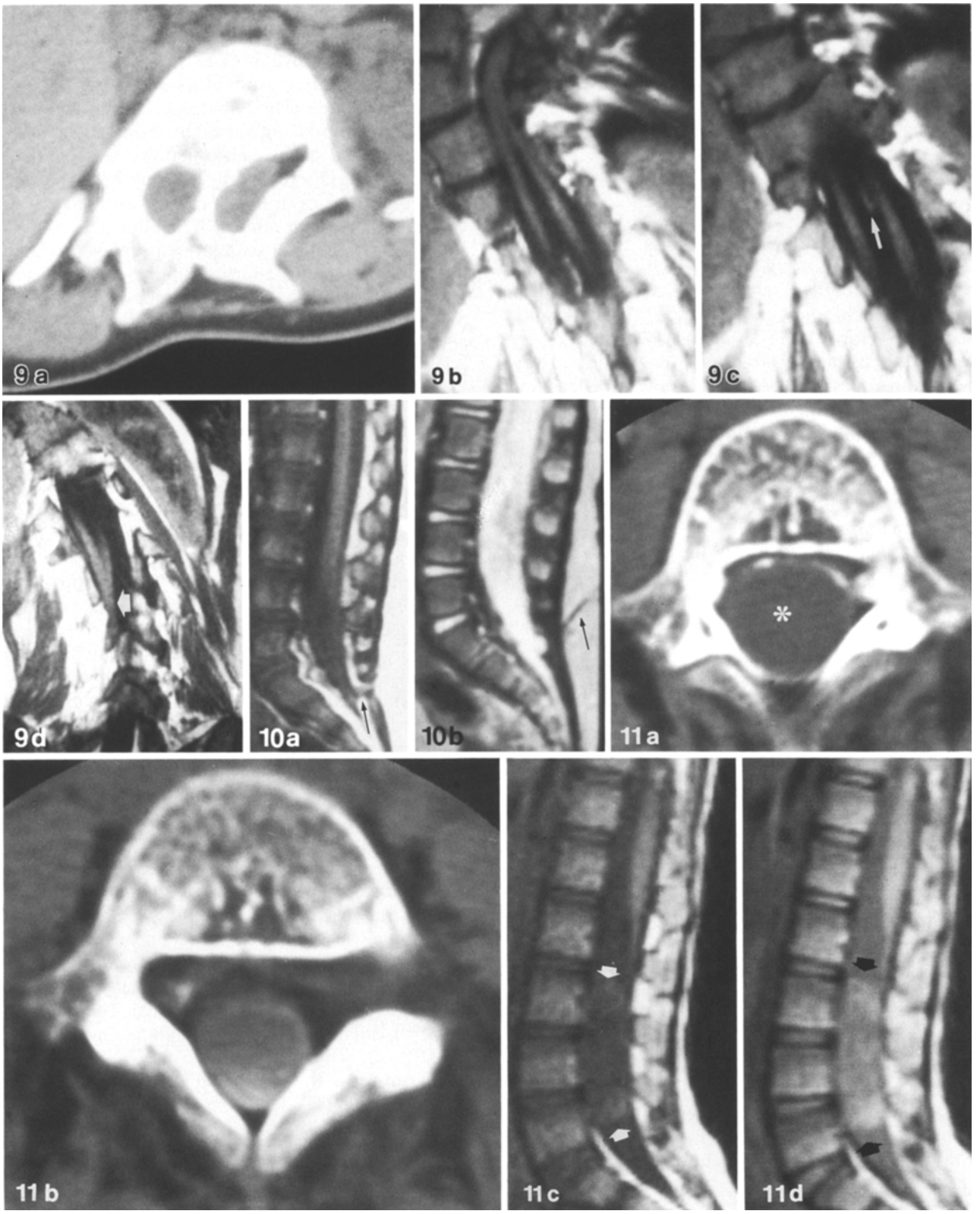

Fig. 9a–d. Diastematomyelia. **a** CT: axial scan. Malformed thoracic vertebra with thick bony spur. **b–d** MR: SE TR 300 – TE 20, coronal scans. Duplication of the spinal cord at the thoracolumbar junction with low tethered cord *(big white arrow)*, oblique bony spur *(white arrow)*

Fig. 10a, b. Dermal sinus and low tethered cord. MR: **a** SE TR 500 TE 30, **b** SE TR 2000 TE 60. Sagittal scans, dermal sinus lying craniocaudally, low tethered cord *(arrows)*

Fig. 11a–d. Dermoid of the cauda equina. **a, b:** Myelo-CT: axial scans. Large hypodense intradural mass *(asterisk)*; small residues of intrathecal contrast medium. Schisis of the posterior arch, dural sac faintly hyperdense **(b)** due to slight diffusion of the contrast medium below the dermoid. **c, d** MR: sagittal scans. **c** TR 450 TE 30. Ovoid lesion, with signal intensity like that of CSF, at L3, L4, L5 *(white arrows)*. **d** TR 750 TE 100. Signal intensity like that of cord parenchyma and greater that that of CSF *(black arrows)*

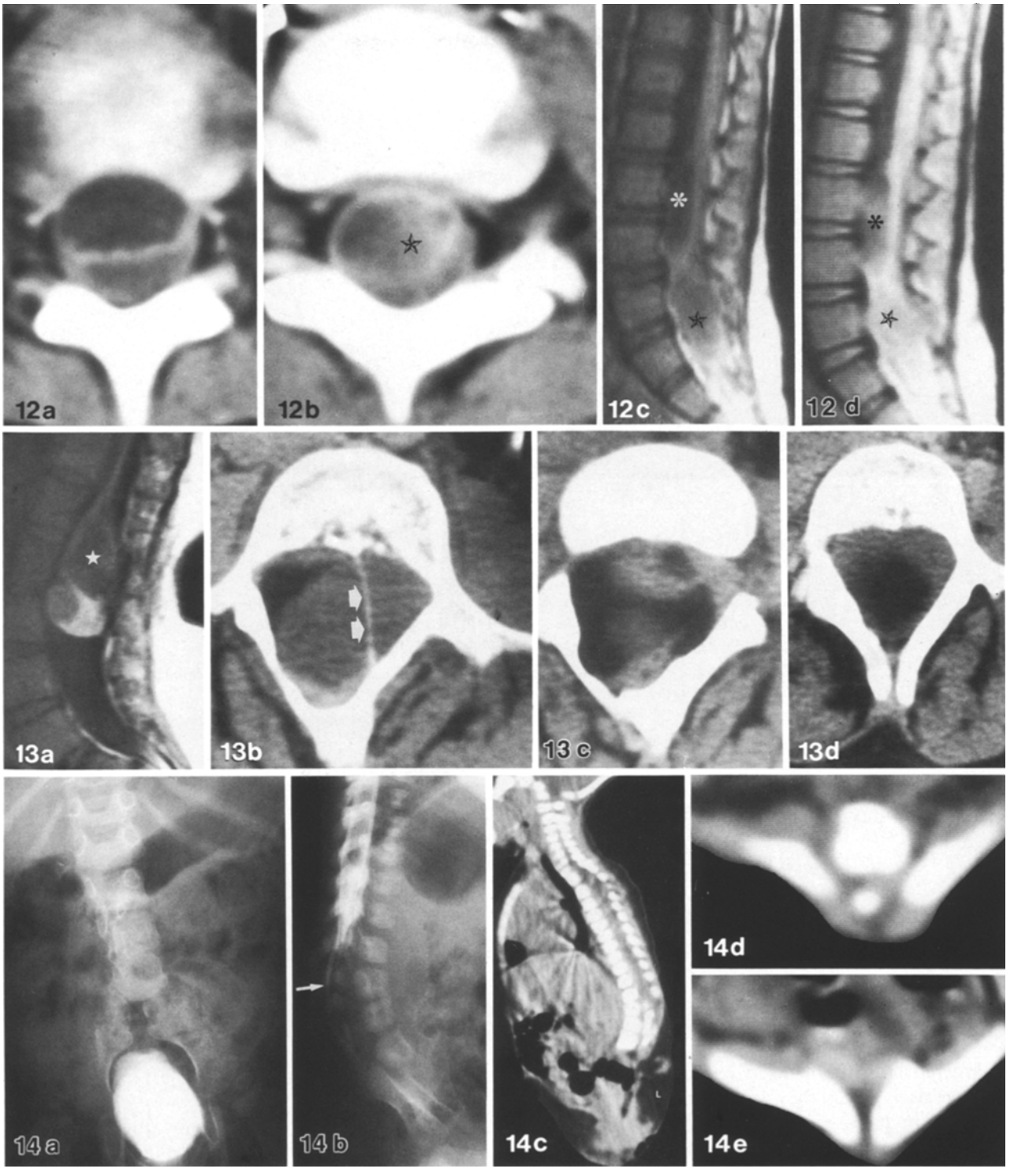

Fig. 12a–d. Dermoid associated with lumbar CSF cyst. **a, b)** CT scan with contrast medium. **a** Rostral scan imaging two intradural areas of different densities surrounded by a hyperdense rim. **b** More caudal scan showing a lesion of increased density *(star)*, bounded by a hyperdense ring, occupyng the greater part of the dural sac. **c, d** MR: sagittal scans. TR 500 TE 30 and TR 1500 TE 70. MR demonstrated the presence of craniad CSF-containing lesion *(asterisk)* and of a second, caudad, lesion attributable to a dermoid *(star)*. Presence of a dermal sinus

Fig. 13a–d. Lumbar teratoma. **a** MR: sagittal scan. TR 500 TE 30. Large mass *(star)* of variable intensity and density to the apex of which the conus is attached; ectasia of the spinal canal and scalloping of the vertebral bodies. **b–d** CT: axial scan. Diastematomyelia suggested by the presence of a bony spur *(arrows)*

Fig. 14a–e. Caudal regression syndrome (type 3). **a** Plain X-ray. Agenesis of L5 and of the sacrum-coccyx. The ilia articulate with the sides of the lowest vertebra present. **b** Myelography. The dural sac stops at L1 level; the root pouches break up in the soft tissues *(arrow)* **c** CT: direct sagittal scan. Dysmorphic lumbar vertebrae. Associated lipoma *(L)*. Thoracolumbar kyphosis. Virtual spinal canal. **d, e** Axial CT. Alae ilii articulate with the last lumbar verebra, spinal canal absent. In the lower scans the alae ilii approach the midline

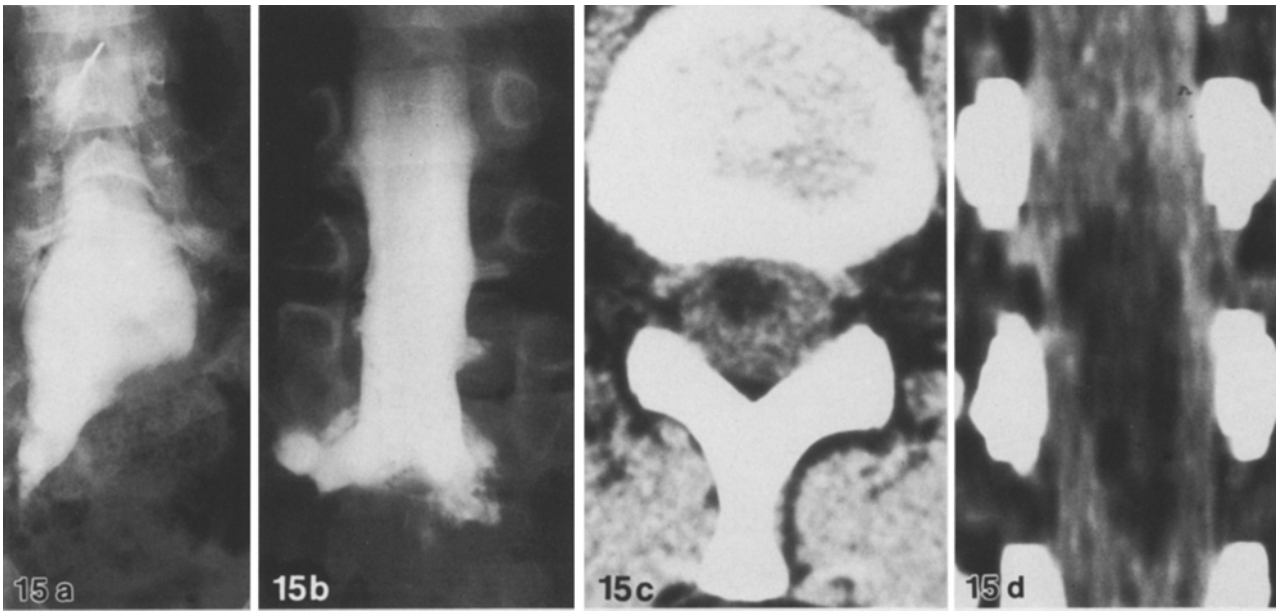

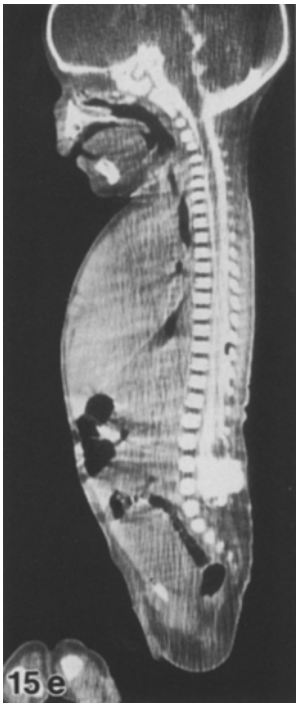

Fig. 15 a–e. Lipoma and tethered cord. **a, b** Myelography. Different patterns of amputation and deformation of the dural sac. **c, d** CT: axial scan and coronal reconstruction. Cervicothoracic intramedullary lipoma. **e** Myelo-CT: direct sagittal scan, lipomyelomeningocele

Fig. 16 a, b. Lipoma and tethered cord. Myelo-CT: axial scan. Probably subpial injection of the contrast medium *(star)*

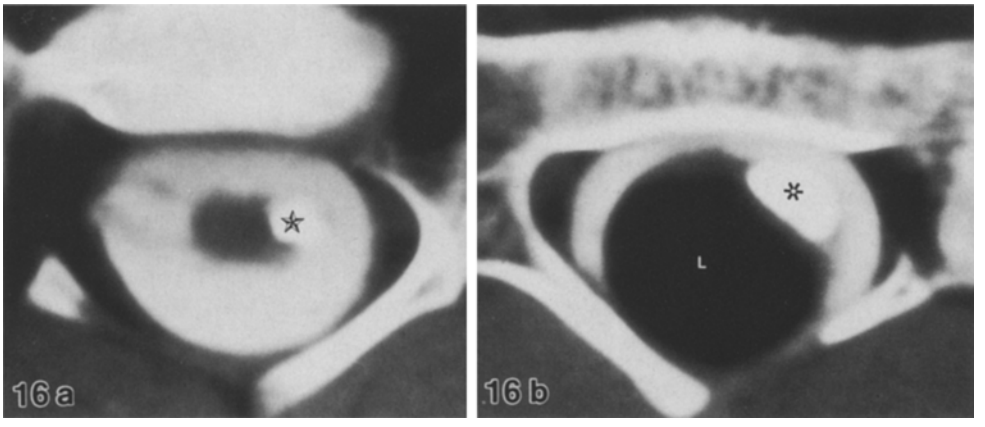

We had a few problems in demonstrating these lesions precisely, when they were associated with other lesions, as in the case in Fig. 12, in which operation revealed a CSF cyst. The variability of signal intensity was due to the variability of the histopathological texture.

Teratoma [51] posed pratically no problems: it is a true tumor, given the almost constant presence of the three constituents of the germ layer, was recognizable both on the MR (Fig. 13 a) and on the CT scans (Fig. 13 b–d). In our case, in addition, MR revealed the close ties between conus and tumor, which proved to be associated with hints of diastematomyelia, like the bony spicule in Fig. 13 b.

In the cases of dermal sinus the fistula was exceedingly hard to detect because of its oblique lie. Detection would be possible only here and there, or if the course were parallel to the planes of study. With sagittal MR scans the problem was overcome.

Caudal regression [55, 56]

The caudal regression syndrome is a very rare version of OSD and is characterized by a series of ab-

normalities including, in a variety of combinations, sirenomelia, lumbosacral agenesis (Fig. 14a), genital malformations, renal dysplasia, anal atresia and pulmonary hypoplasia [1]. The disturbance of embryogenesis occurs before the 4th week. Our case may be classified as a type III dysgenesis (21%) in the classification proposed by Renshaw [56] in 1978, associated with a large subcutaneous lipoma (Fig. 14b–e).

Conclusions

In the pre-CT era the combination of a precise clinical pattern with X-ray images of the spine could prompt a suspicion of OSD. The suspicion inevitably led to the performance of a myelogram, which as inevitably supplied an incomplete picture of the malformation (Fig. 15a, b).

A standard CT scan together with reconstructions allowed good discrimination of the bony structures, fair visualization of a lipoma and only a vague picture of the cord and root components (Fig. 15c, d). Intrathecal contrast (myelo-CT) supplemented, when possible, by direct sagittal scans, permitted closer analysis of the connexions among the various components of the malformation (Fig. 15e).

With MR an accurate and almost complete study can be made of these lesions in all their complexity (Fig. 8), thus obviating the risk of puncturing a malpositioned cord (Fig. 16a, b). CT maintains its advantage and is still crucial to the evaluation of the bony landmarks. The greater the anatomical complexity of a dysraphism, the greater the advantage of combining MR and myelo-CT. Even so, some features of a malformation may still be far from clear. As reported by Dachling Pang, there is, for example, no solution as yet to the problem of discriminating the conus from the thickened filum terminale in some versions of the tethered cord syndrome. In such cases the surgeon is faced with the same problem even with the operating microscope. It would seem appropriate, indeed, to call the combination of conus-thickened filum terminale "neurofibrous structure".

Apart from such extreme cases, it is now possible, through the advances made by neuroradiological procedures, to reach a precise radiological diagnosis of OSD and so arrive at a better preoperative appraisal and more satisfactory clinical results.

References

1. Naidich TP, McLone DG, Harwood-Nash (1983) Spinal dysraphysm. In: Newton TH, Potts DG (eds) Computed tomography of the spine and spinal cord. Clavadel Press, San Anselmo, Calif., p 299
2. Harwood-Nash DC (1981) Computed tomography of the pediatric spine: a protocol for the 1980's. Radiol Clin North Am 19: 479–494
3. Rejo IM, Harwood-Nash (1978) Computed tomography metrizamide myelography in spina dysraphism in infants and children J Comput Assist Tomogr 2: 549
4. Naidich TP, Harwood-Nash DC, McLone DG (1982) Radiology of spinal dysraphism. Clin Neurosurg 30: 341–365
5. Haughton VM (1988) Spinal cord diseases. Presented at the 74th Scientific Assembly and Annual Meeting of RSNA, November 27–December 2, 1988. Radiology 169 [Suppl]: 127
6. Williams AL, Quencer RM (1988) The abnormal spinal cord: current imaging status. Presented at the 74th Scientific Assembly and Annual Meeting of RSNA, November 27–December 2, 1988. Radiology 169 [Suppl]: 284
7. Zimmermann RA (1988) Pediatric central nervous system. Presented at the 74th Scientific Assembly and Annual Meeting of RSNA, November 27–December 2, 1988. Radiology 169 [Suppl]: 127
8. Naidich TP, Barrovich AJ (1988) Pediatric neuroradiology: the maturing central nervous system. Presented at the 74th Scientific Assembly and Annual Meeting of RSNA, November 27–December 2, 1988. Radiology 169 [Suppl]: 295
9. Han JS, Benson JE, Kaufman B et al. (1983) NMR imaging of the spine, AJNR 4: 1151
10. Modic MT, Weinstein MA, Pavlicek W et al. (1983) Nuclear magnetic resonance imaging of the spine. Radiology 148: 757
11. Barnes PD, Lester PD, Iamanashy WS, Prince GR (1986) Magnetic resonance imaging in infants and children with spinal dysraphism. AJNR 7: 465
12. Norman D, Mills CM, Brant Zawadzky M et al. (1984) Magnetic resonance imaging of the spinal cord and canal. Potentials and limitations. AJNR 5: 9
13. Roos RAC, Vielvoye GJ, Voormolen JHC, Peters ACB (1986) Magnetic resonance imaging in occult spinal dysraphism. Pediatr Radiol 16: 412–416
14. Altman NR, Altman DH (1986) MR imaging of spinal dysraphism. AJNR 8: 533–538
15. Flanningan – Sprague BD, Modic MT (1988) The pediatric spine: normal anatomy and spinal dysraphism. In: Modic MT, Masarik TJ, Ross JS (eds). Magnetic resonance imaging of the spine. Year Book Medical Publishers, Chicago London Boca Rathon, pp 240–256
16. Norman D (1986) The spine In: Brant-Zawatzky M, Norma D (eds) Magnetic resonance imaging of the central nervous system. Raven Press, New York, pp 289–328
17. Davis PC, Hoffman JC, Turner JR et al. (1988) Spinal abnormalities in pediatric patients: MR imaging findings compared with clinical myelographic and surgical findings. Radiology 166: 679–685
18. French BN (1982) Midline fusion defects of formation. Neurol Surg 2: 1236
19. Creissard P, Redondo A (1974) Spina bifida. Neurologie 4: 39
20. Anderson FM (1975) Occult spinal dysraphism: a series of 73 cases. Pediatrics 55: 826
21. O'Railly R, Muller F (1986) The normal and abnormal development of the nervous system in the early human embryo J Pediatr Neuroscience 2: 89
22. French BN (1982) The embryology of spinal dysraphism. Clin Neurosurg 30: 295–340
23. McLone DG, Mutluer S, Naidich TP (1983) Lipomeningoceles of the conus medullaris. Concepts Pediatr Neurosurg 3: 170
24. Matson DD (1969) Neurosurgery in infancy and childhood, 2nd edn. Complete revision of monograph by Ingraham FD, Matson DD. Thomas, Springfield

25. Humphreys RP (1985) Spinal dysraphism. In: Wilkins RH, Rengachary SS (eds) Neurosurgery. McGraw-Hill, New York, pp 2041-2052
26. Page LK (1985) Occult spinal dysraphism and related disorders. In: Wilkins RH, Rengachary SS (eds) Neurosurgery. McGraw-Hill, New York, pp 2053-2058
27. Hoffman HJ, Taecholarn C, Hendrick EB, Humphreys RP (1985) Management of lipomyelomeningoceles: experience at the hospital for sick children Toronto. J Pediatr Neurosciences 1: 3
28. Giuffrè R (1966) Intradural spinal lipomas. Acta Neurol Chir 14: 69-95
29. Emery JL, Lendon RG (1969) Lipomas of the cauda equina and other fatty tumours related to neurospinal dysraphism. Dev Med Child Neurol [Suppl] 11: 62-70
30. Chapman PH (1982) Congenital intraspinal lipomas. Anatomic considerations and surgical treatment. Child's Brain 9: 37-47
31. Cotroneo E, Floris R (1987) MRI of lumbosacral lipoma. In: Calabro A, Leonardi M (eds) Computer Aided Neuroradiology. XIVth Congress of the European Society of Neuroradiology, Udine, Italy, September 8-12. Ed. Internazionali, Rome
32. Bruce DA, Schut L (1979) Spinal lipomas in infancy and childhood. Child's Brain 5: 192-203
33. Dossetor RS, Kaiser M, Veiga-Pires JA (1979) CT scanning in two cases of lipoma of the spinal cord. Clin Radiol 30: 227-331
34. Walsh JW, Markesbery WR (1980) Histological features of congenital lipomas of the lower spinal canal. J Neurosurg 52: 564-569
35. Wippold FJ, Citrin C, Barkovich AJ, Sherman (1987) Evaluation of MR in spinal dysraphism with lipoma: comparison with metrizamide computed tomography. Pediatr Radiol 17: 184-188
36. Sarwar M, Virapongse C, Bhimani S (1984) Primary tethered cord syndrome: a new hypothesis of its origin. AJNR 5: 235-242
37. Lapras C, Patet JD, Mottolese C (1988) Le syndrome de traction du cone terminal: Moelle attache et lipomes sacres. Neurochirurgie 34 [Suppl 1]: 91
38. Hoffman HJ, Hendrick EB, Humphrey RP (1976) The tethered spinal cord: its protean manifestations, diagnosis and surgical correction. Child's Brain 2: 145-155
39. Kaplan JO, Quencer MR (1980) The occult tethered conus syndrome in the adult. Radiology 137: 387-391
40. Fitz CR, Harwood-Nash DC (1975) The tethered conus. AJR 125: 515-523
41. Dachling Pang, Wilberg JE (1982) Tethered cord syndrome in adults. J Neurosurg 57: 32-47
42. Sarwar M, Crelin ES, Kier EL, Virapongse C (1983) Experimental cord stretchability and the tethered cord syndrome. AJNR 4: 641-643
43. Naidich TP, McLone DG, Mutluer S (1983) A new understanding of dorsal dysraphism with lipoma (lipomyeloschisis). AJNR 4: 103-116
44. Naidich TP, Harwood-Nash (1983) Diastematomyelia: Hemicord and meningeal sheaths; single and double arachnoid and dural tubes. AJNR 4: 633-636
45. Han JS, Benson JE, Kaufman B et al. (1985) Demonstration of diastematomyelia and associated abnormalities with MR imaging. AJNR 6: 215
46. Scotti G, Musgrave MA, Harwood-Nash DC et al. (1980) Diastematomyelia in children metrizamide and CT metrizamide myelography. AJR 135: 1225-1232
47. Guthkelch AN (1985) Diastematomyelia. In: Wilkins RH, Rengachary SS (eds) Neurosurgery. McGraw-Hill, New York, pp 2058-2061
48. Frerebeau P, Dimeglio A, Gras A, Harbi H (1984) Diastematomyelia. Report of 21 cases surgically trated by a neurological and orthopedic team. Child's Brain 10: 328
49. Naidich TP, Regenbogen V, Limauro D, McLone DG (1988) Presented at 26th Annual Meeting of the American Society of Neuroradiology, Chicago, March 15-20, 1988
50. Gerlach J (1978) Dermal sinuses and dermoids. In: Vinken PJ, Bruyn GW (eds) Handbook of clinical neurology, vol 32. Elsevier, Amsterdam, New York, pp 449-463
51. Monajati A, Spitzer RM, Larue Wiley J, Heggeness L (1986) MR imaging of a spinal teratoma. J Comput Assist Tomogr 10: 307-310
52. Bucy PC, Buchanan DN (1935) Teratoma of spinal cord. Surg Cynecol Obstet 60: 1137-1144
53. Scotti G, Harwood-Nash DC, Hoffman HJ (1980) Congenital thoracic dermal sinus: diagnosis by computer assisted metrizamide myelography. J Comput Assist Tomogr 4: 675-677
54. List CF (1941) Intraspinal epidermoids, dermoids and dermal sinuses. Surg Gynecol Obstet 73: 525-538
55. Dachling Pang, Hoffman HJ (1980) Sacral agenesis with progressive neurological deficit. Neurosurgery 7: 118-126
56. Renshaw TS (1978) Sacral agenesis: a classification and review of 23 cases. J Bone Joint Surg (Am) 60A: 373-383

Received: 9 March 1989

Dr. P. Tortori-Donati
Serv. di Neuroradiologia
Ospedale San Martino
16132 Genova
Italy